

IEICE **TRANSACTIONS**

on Communications

VOL. E102-B NO. 6
JUNE 2019

The usage of this PDF file must comply with the IEICE Provisions on Copyright.

The author(s) can distribute this PDF file for research and educational (nonprofit) purposes only.

Distribution by anyone other than the author(s) is prohibited.

A PUBLICATION OF THE COMMUNICATIONS SOCIETY



The Institute of Electronics, Information and Communication Engineers
Kikai-Shinko-Kaikan Bldg., 5-8, Shibakoen 3chome, Minato-ku, TOKYO, 105-0011 JAPAN

Dependable Wireless Feedback Loop Control Schemes Considering Errors and Delay in Sensing Data and Control Command Packets

Satoshi SEIMIYA[†], *Nonmember*, Takumi KOBAYASHI^{†a)}, *Member*, and Ryuji KOHNO[†], *Fellow*

SUMMARY In this study, under the assumption that a robot (1) has a remotely controllable yawing camera and (2) moves in a uniform linear motion, we propose and investigate how to improve the target recognition rate with the camera, by using wireless feedback loop control. We derive the allowable data rate theoretically, and, from the viewpoint of error and delay control, we propose and evaluate QoS-Hybrid ARQ schemes under data rate constraints. Specifically, the theoretical analyses derive the maximum data rate for sensing and control based on the channel capacity is derived with the Shannon-Hartley theorem and the path-loss channel model inside the human body, i.e. CM2 in IEEE 802.15.6 standard. Then, the adaptive error and delay control schemes, i.e. QoS-HARQ, are proposed considering the two constraints: the maximum data rate and the velocity of the camera's movement. For the performance evaluations, with the 3D robot simulator GAZEBO, we evaluated our proposed schemes in the two scenarios: the static environment and the dynamic environment. The results yield insights into how to improve the recognition rate considerably in each situation.

key words: wireless visual feedback loop control, wireless capsule endoscopy, IEEE 802.15.6, QoS-Hybrid ARQ, allowable FPS

1. Introduction

A wireless capsule endoscopy (WCE) is one of typical highlights of medical ICT, that is a state of the arts of wireless information and communication technology (ICT) for medicine and healthcare. Beyond WCE, a micro size of implant robot, which can move to investigate with vital sensors, e.g. an image sensor or a camera; and actuators, e.g. micro pincettes, laser; inside a body, e.g. intestine and blood vessel, has been studied and developed. It works not only like a usual capsule endoscope but also like a surgical robot and a drug delivery robot. It takes movies inside the body, controls its manipulator to cut off polyps, and delivers drugs to the target areas. To realize such a robot, the wireless feedback loop control, the technology that enables mutual and real-time communication between an implant device and an outside controller, is very important.

Communications theory and control theory have traditionally been related to each other. However, for last two decades, communications theory has been mainly concerned with the reliable transmission of information from one point to another, and is relatively indifferent to the specific purpose of the transmitted information and whether it is eventually fed back to the source. Control theory, in contrast, has been

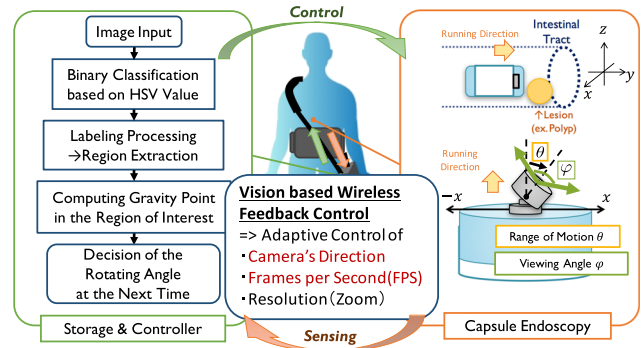


Fig. 1 Key concept of our research.

concerned mainly with using information in a feedback loop to achieve some performance object, and usually assumes that communication link limitations do not affect performance significantly. In systems with large communication bandwidth, it makes sense to treat communication and control as independent functions, since the analysis and design of the overall system is simplified [1].

However, although some researchers have been trying to introduce the ultra wide-band (UWB) technology into implantable devices [2]–[4], in Japan, the current upper limit of the communication bandwidth for WCE is 300 [kHz] [5]. This can introduce large quantization errors that affect control performance, due to the low resolution of the transmitted data. Therefore, feedback loop control under data rate constraints is valuable for stable operation considering the errors present in band-limited channels. Not only that, the environment around the capsule changes time to time because the robot is carried by peristalsis through the digestive tract. Thus, it is important for practical use of the system to define some QoS (Quality of Service) levels and to change its image acquisition schemes and error control methods.

Considering those requirements for the next generation WCE, in this study, we propose the vision based wireless feedback loop control system shown in Fig. 1. The flow of operations is as follows.

- (Step 1) The swingable camera on the head of the pill captures an image.
- (Step 2) The RF module in the pill transmits the image to the 'Storage & Controller' outside the body.
- (Step 3) The controller does the image processing, and judges whether there is a region of interest or not.
- (Step 4) If the region of interest is reflected in the image,

Manuscript received July 2, 2018.

Manuscript revised October 22, 2018.

Manuscript publicized December 19, 2018.

[†]The authors are with the Yokohama National University, Yokohama-shi, 240-8501 Japan.

a) E-mail: kobayashi-takumi-ch@ynu.jp

DOI: 10.1587/transcom.2018HMP0008

the controller sends ACK[†] and control commands to change parameters to focus on it. Otherwise, the controller sends NAK^{††}

- (Step 5) The WCE receives the control command with ACK / NAK, and it changes its camera's parameters.
- (Step 6) Back to the Step 1 and repeat the Step 1-5 until the inspection is finished.

This paper is organized as follows. In Sect. 2, we describe the details of our proposed vision based wireless feedback loop control system. In Sect. 3, we are going to see the uplink communication in our proposed feedback loop control system from the viewpoints of information theory, and find out the allowable FPS(=aFPS). Within the aFPS, we regard the image transmission is done ideally. In Sect. 4, we are going to see the downlink communication and show the adaptive error control and delay control schemes, which are specific to the proposed system. In Sect. 5, the proposed error control and delay control schemes under the constraints are evaluated with the prototyped camera in the Gazebo. Finally, Sect. 6 concludes this paper.

2. Proposed Visual Information Based Wireless Feedback Loop Control System for the Next Generation WCE

This section describes the concept and process of our proposal shown in Fig. 1.

2.1 Overview of the Proposed Next Generation WCE System

Figure 1 shown in Sect. 1 can be replaced by Fig. 2.

In the figure, each line corresponds to as follows.

- Green-Colored Solid Line ⇔ Channel for Controlling Command Packets
- Green-Colored Broken Line ⇔ Channel for ACK/NAK Signal of Controlling Command Packets
- Orange-Colored Solid Line ⇔ Channel for Sensing Data Packets
- Orange-Colored Broken Line ⇔ Channel for ACK/NAK Signal of Sensing Data Packets

The aim of this system is to find the target lesion (at here, the spherical object like a polyp) and to focus on it as much as possible, effectively.

There is a limit on the amount of available energy devoted to the acquisition of picture. Therefore, we also would like to propose the two modes, 'Search Mode' and 'Focus Mode' shown in Fig. 3.

2.1.1 Search Mode

In this mode, the WCE takes a picture at a certain interval,

[†]ACK: the signal to notice that the transmitted data is received correctly

^{††}NAK: the signal to notice that the transmitted data is received with errors or lost

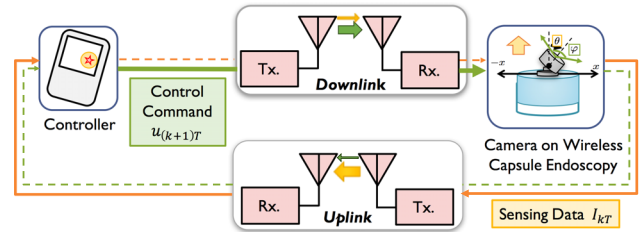


Fig. 2 Proposed vision based wireless feedback loop control system for the next generation WCE.

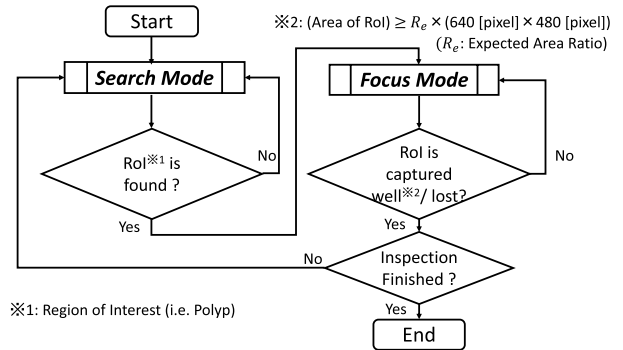


Fig. 3 Flow chart of the proposed examination.

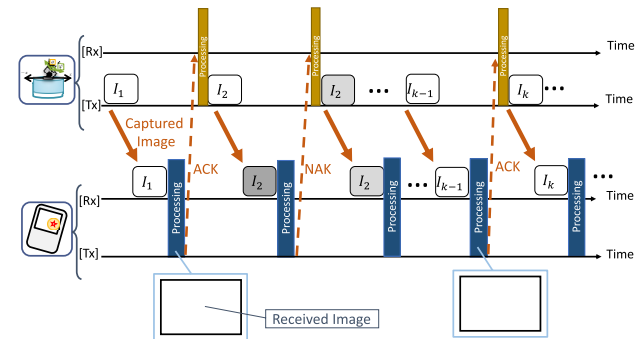


Fig. 4 The sequence diagram of the 'Search Mode'.

and transmits the image to the antenna around the body. This mode will last until an ROI is reflected in a captured frame. Its sequence diagram is illustrated in Fig. 4.

2.1.2 Focus Mode

After finding out the region of interest, the system moves to the 'Focus Mode.' Its sequence diagram is illustrated in Fig. 5.

2.2 Assumed Data Packets' Structures

2.2.1 Data in Uplink (Sensing Data)

In this study, the sensing data means the image taken by the camera on WCE. We assume that the image format is the BMP file format for the simplification, like shown in Fig. 6.

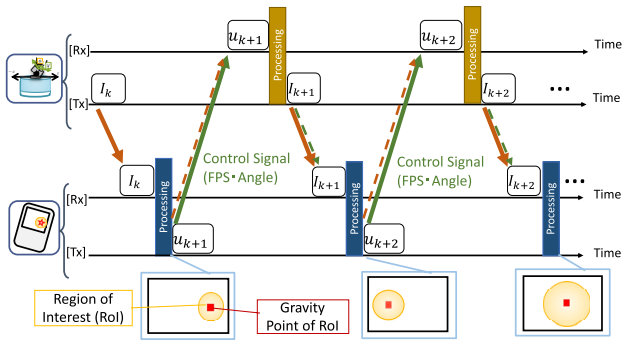


Fig. 5 The sequence diagram of the 'Focus Mode'.

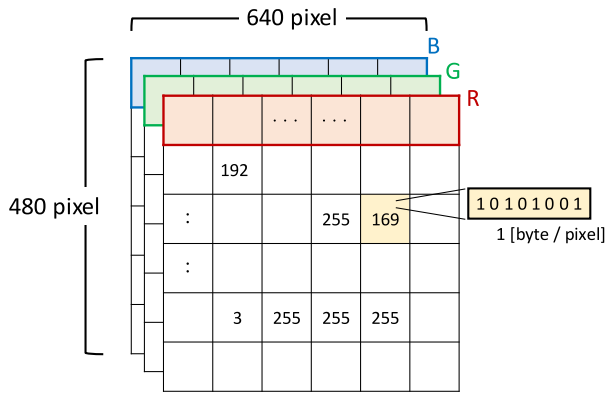


Fig. 6 BMP image structure.

To consider the image transmission in the proposed system, with the knowledge of the Medical ICT Group in National Institute of Information and Communications Technology (NICT) [6], we use the distributed video coding, which can shift the complexity of coding and decoding to the receiver side. The details are as follows.

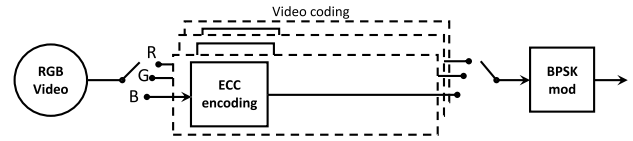
2.2.2 Encoding

Figure 7(a) and Fig. 7(b) show procedures of the video encoding and decoding method. The original RGB image is encoded separately in each color component through the same procedure.

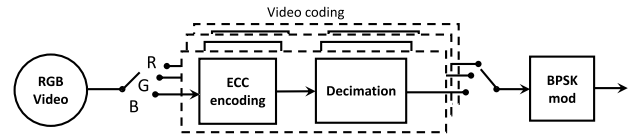
The amplitude of each color component in every pixel is quantized in N_B bits. The quantized bits in the i th frame image are denoted as $b_{x,y,k}^i$, where $x \in \{1, \dots, x_{max}\}$ and $y \in \{1, \dots, y_{max}\}$ respectively stand for the horizontal and vertical index of the pixel, and $k \in \{1, \dots, N_B\}$ represents the bit-depth of the pixel. The frame image is also represented by $\mathbf{B}^i = \{\mathbf{b}_{1,1}^i, \dots, \mathbf{b}_{x,y}^i, \dots, \mathbf{b}_{x_{max},y_{max}}^i\}$ where $\mathbf{b}_{x,y}^i = \{b_{x,y,1}^i, \dots, b_{x,y,N_B}^i\}$. This frame image is encoded at the Error Correction Coding (ECC) encoder in the following order:

$$\mathbf{B}_{ecc}^i = \{\mathbf{b}^i(0), \dots, \mathbf{b}^i(n), \dots, \mathbf{b}^i(x_{max} \cdot y_{max} - 1)\} \quad (1)$$

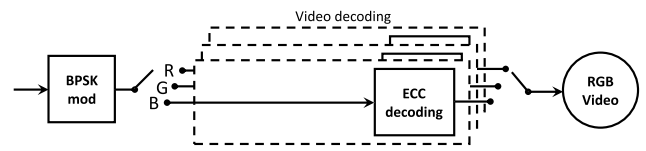
where



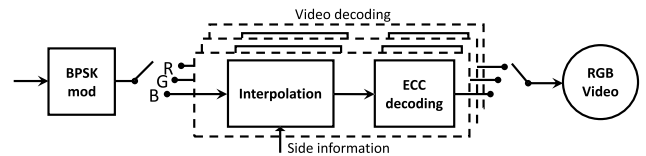
(a) Encoder for the initial frame



(b) Encoder for the successive frames



(c) Decoder for the initial frame



(d) Decoder for the successive frames

Fig. 7 Distributed video coding and decoding procedures.

$$\mathbf{b}^i(n) = \mathbf{b}_{x_n, y_n}^i$$

$$y_i = \text{rem}(\text{floor}(n, x_{max}) + \text{rem}(n, y_{max}), y_{max}) + 1$$

At here, $\text{rem}(n, m)$ is the remainder of n divided by m , and $\text{floor}(n, m)$ is the largest integer less than ' n divided by m .' The bit sequence \mathbf{B}_{ecc}^i is encoded by L_{info} bits, and then N_w codewords with a length of L_{ecc} bits are obtained. In the paper [6], a systematic linear code, which is separable into information and its redundant parts, is used as ECC since a reduction of the number of transmitting bits is easily implemented by a simple decimation; thus, for the initial frame, both the information bits \mathbf{B}_{ecc}^i and parity bits are transmitted. On the other hand, only the parity bits are transmitted for the successive frames. By using this encoding method, the total compression rate R is given by

$$R = \frac{1}{N_f} \left\{ \frac{1}{R_c} + (N_f - 1) \left(\frac{1}{R_c} - 1 \right) \right\} \quad (2)$$

where N_f is the number of frames to be encoded, and R_c is the coding rate of the employed ECC represented by Eq. (3).

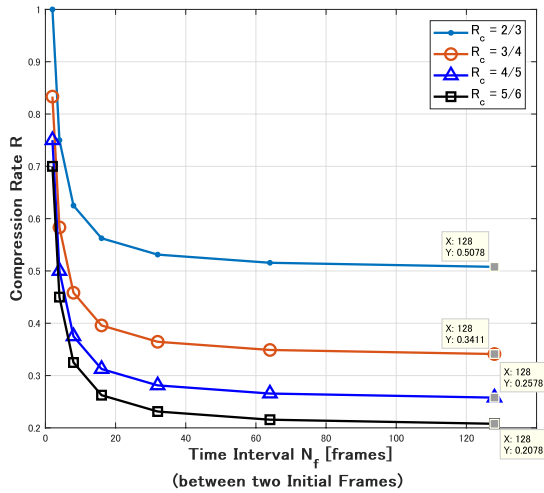


Fig. 8 Compression rate R in each code rate.

FPS(32bits)	Camera Angle (32bits)	CRC (16bits)
-------------	-----------------------	--------------

Fig. 9 Control command packet structure.

$$R_c = \frac{x_{max} \cdot y_{max} \cdot N_B}{N_w \cdot L_{ecc}} \quad (3)$$

Therefore, from the Eq. (2), we can say that the total compression rate R depends on the coding rate R_c and the number of frames N_f . The characteristic curve is shown in Fig. 8.

2.2.3 Decoding

Figure 7(c) and Fig. 7(d) also show the decoding procedure. For the initial frame, ordinary decoding using ECC is applied. For the successive frames, in which received codewords contain only their parity bits, frame images are estimated by using the previous frame image and a correlation characteristic between successive frames as side information. In this study, to focus on the communication schemes, we would like to skip the details of the motion estimation.

2.2.4 Data in Downlink (Control Command)

The data in downlink are the camera's angle and FPS. The packet structure of control command is illustrated in Fig. 9. Those information are represented with the IEEE 754 standard [7].

2.3 Assumed Channel Model for Implant BAN

To consider the wireless feedback system in Implant Body Area Networks, we also have to think about how to describe the complex channel model. In this study, based on the time-varying SNR model which we derived in [8] using the NIST implant propagation model [9] and assuming that the propagation distance between WCE inside the human body and the controller outside the human body is 10 [cm],

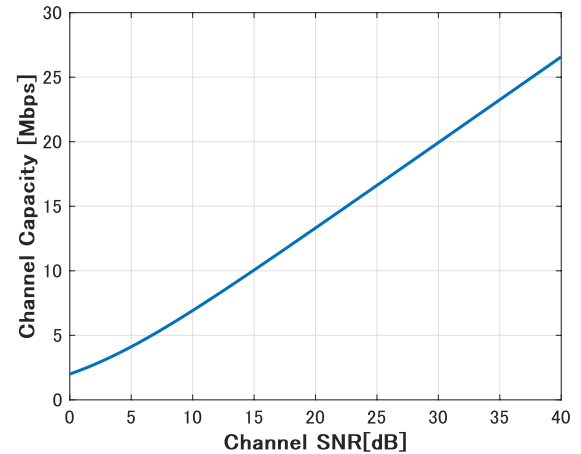


Fig. 10 Channel capacity in each SNR for the proposed System (Fig. 2).

we set the SNR for the AWGN channel in the performance evaluations as 3 [dB].

3. Theoretical Analysis for the Allowable FPS Derivation

This section derives the constrains in the proposed system.

3.1 Derivation of the Channel Capacity in the Proposed System

For the general wireless feedback systems, we can use either the half-duplex or the full-duplex communication. However, the size of the wireless capsule endoscopy is limited, so from the practical point of view, we are going to use the half-duplex communication system in our proposed system.

The Shannon-Hartley theorem states that the channel capacity is given by

$$C = B \log_2 \left(1 + \frac{S}{N} \right) \quad (4)$$

where C is the capacity in bits per second, B is the bandwidth of the channel in Hertz, and S/N is the signal-to-noise ratio. The signal-to-noise ratio(SNR) of the wireless channel has already been derived in [8]. In addition, referring to the commercial product by Given Imaging Ltd., the frequency band f and the bandwidth B can be set as $f = 433$ [MHz] and $B = 2$ [MHz] [10]. Therefore, the channel capacity in our proposed system can be illustrated like Fig. 10.

3.2 Allowable FPS (=aFPS) Derivation

In the proposed wireless feedback loop control system, the amount of data in uplink communication is much more than that in downlink. Therefore, the channel capacity derived at the former section mainly affects the allowable FPS (from here, in short, aFPS) of the camera on the wireless capsule endoscopy. The aFPS can be derived as follow:

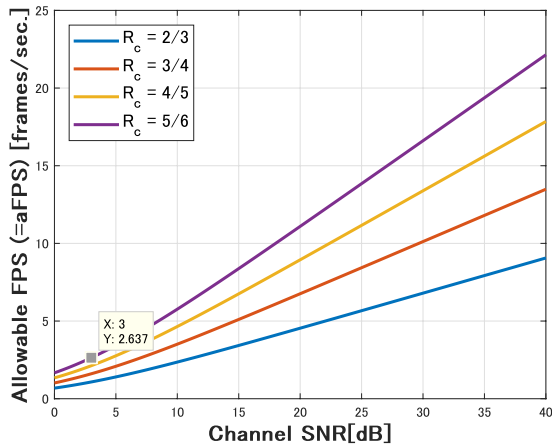


Fig. 11 Allowable FPS values in each channel SNR.

$$\text{aFPS}(R_c, SNR) = \frac{C(SNR)}{M \cdot R(R_c)}, \quad (5)$$

where $C(SNR)$ is the channel capacity in a certain SNR, M denotes the size of an Image (= 722 [kbytes], as shown in Fig. 6), and the $R(R_c)$ denotes the compression ratio expressed by Eq. (2) with the assumption of $N_f = 2$. The characteristic curve of it is illustrated in Fig. 11. In the following performance evaluations, we assume that (1) the code rate R_c for protecting the image transmitted through the uplink is $5/6$, and (2) there is no communication error in the uplink when the picture is taken under the FPS 2.637.

4. Proposed Adaptive Error Control and Delay Control

This section describes the proposed error control and delay control.

4.1 Proposed QoS-Based ‘Error’ Control Scheme

This subsection describes our proposed adaptive ‘error’ control scheme. In general, the less the code rate is, the more protected the code is. However, when we assume to use the punctured convolutional code, the less the code rate is, the less the throughput becomes. From this point of view, we propose to change the code rate depending of the stability.

4.1.1 [Proposal A] RoI (Region of Interest) Position Based Error Control

The first strategy for error control is to change the code rate of punctured convolutional code which protects the control command packets in downlink, depending on the position of the target object. Its concept is illustrated in Fig. 12. In this figure, the black-colored object means the region of interests (RoI), and the red-colored square is the gravity point (=feature point) of RoI. After receiving an image from the camera, the controller extracts feature point [12]. Based on the position information, the controller decides the code rate to protect the control command packets. In this paper, we divided the region into three areas illustrated in Fig. 12.

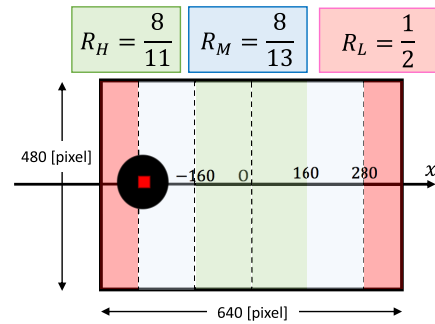


Fig. 12 QoS definitions in proposed ‘Error’ control scheme.

4.2 Proposed QoS-Based ‘Delay’ Control Scheme

Usually, the more pictures the robot sends, the more energy it needs. To reduce the unnecessary capturing is important for a battery driven robot, so we are going to describe our proposed adaptive ‘delay’ control scheme.

4.2.1 [Proposal B] Capturing Interval Control Between Search Mode and Focus Mode

The strategy for delay control is to change the capturing interval (=FPS) depending on whether the region of interested is reflected on an image or not. When RoI is not in the captured image, the controller sends the controlling command packets with FPS=0.5 to save battery. If there is the RoI, and its size is more than 2% in the captured image, the controller send the controlling command packets with FPS=2.5.

5. Total Performance Evaluations Considering Both Error and Delay with the Prototyped Camera in the Gazebo

This section evaluates our proposed error and delay control schemes from practical point of view with the prototyped camera in the 3D robot simulator, Gazebo. In the evaluation, if we do the performance evaluation only in the dynamic environment, when the camera misses the targeting object, the reason of it cannot be determined, because there are two conceivable causes, (1) communication error or (2) insufficient capturing interval. Therefore, we did the evaluation for each proposal, respectively.

5.1 Simulation Environment

5.1.1 Common Platform among Evaluations

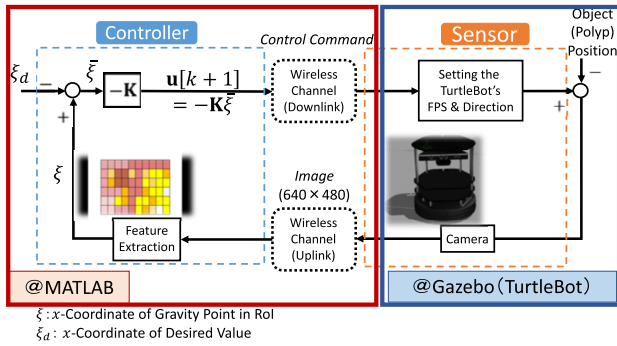
In the following simulations, we are going to use the feedback system illustrated in Fig. 13. In the downlink, the camera’s direction at the discrete time $k + 1$ expressed as $u[k + 1]$ is derived as follows;

$$u[k + 1] = -\mathbf{K}\tilde{\xi} = -\mathbf{K}(\xi - \xi_d) \quad (6)$$

where \mathbf{K} is the proportional gain, ξ is the x-coordinate of the

Table 1 Parameters of the wireless communication department.

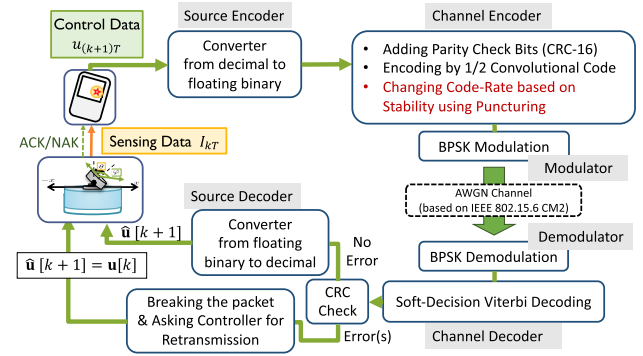
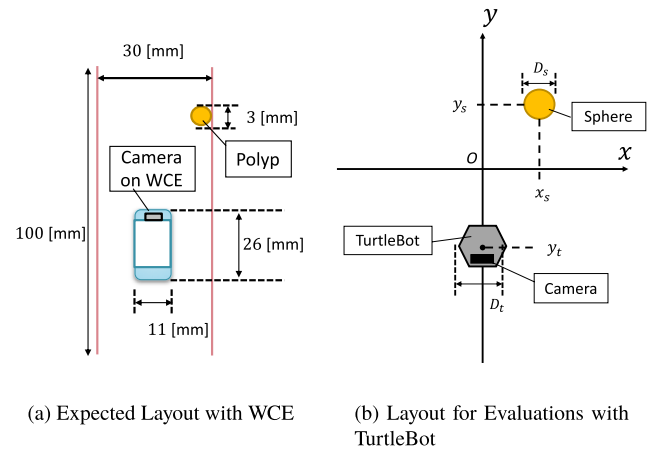
Modulation Scheme	BPSK
Encoder	(5,7) Convolutional Encoder
Original code rate	$R_L = 1/2$
Constraint Length k	3
Cycle of Puncturing	8
Puncturing Matrix for $R_M = 8/13$	$\begin{bmatrix} 1 & 1 & 0 & 1 & 0 & 0 & 1 & 1 \\ 1 & 1 & 1 & 1 & 1 & 1 & 1 & 1 \end{bmatrix}$
Puncturing Matrix for $R_H = 8/11$	$\begin{bmatrix} 1 & 0 & 1 & 1 & 0 & 0 & 1 & 1 \\ 1 & 1 & 1 & 1 & 1 & 1 & 0 & 0 \end{bmatrix}$
CRC Encoder	CRC-CCITT
Decoder	Soft-Decision Viterbi Decoding
Max. Number of Retransmissions	Not Limited
Wireless Channel	AWGN[8]
Packet Length	64 bit (FPS:32bit + Angle:32bit [7])
ARQ protocol	Stop-and-wait ARQ
Propagation Distance d	10 [cm] [8]
Signal Bandwidth B	2 [MHz]

**Fig. 13** Control department of the proposed feedback system.

RoI's feature point, and ξ_d is the desired value of ξ . We set 0 to ξ_d , because capturing the target object at the center of the image is a key issue, and we set $1/320$ to \mathbf{K} , considering the fact that the maximum value of $|\xi - \xi_d|$ is 320 [pixel]. The objective of the feedback process in the paper is to get the ξ to 0 as close as possible. We use the 3D simulator 'Gazebo,' which is also used as a development tool for DARPA Robotics Challenge [11]. In the Gazebo, we placed a robot called 'TurtleBot,' having an RGB camera. The image captured in a certain time interval (FPS) comes up to the MATLAB, and the MATLAB does the image processing as described in [12]. In fact, the reflection on the walls around the WCE affects the performance of RoI extractions, but in this performance evaluations, we ignored it, so we omitted walls in Fig. 15(b) and Fig. 15(b).

5.1.2 [Scenario#1] Target Recognition Under the Static Environment

The layout of the robot and a target object is illustrated in Fig. 15(b). To correspond to the expected layout in the actual environment shown in Fig. 15(a) [14], we derive the variables in Fig. 15(a) by scaling up the variables in Fig. 15(a). In fact,

**Fig. 14** Wireless communication department for total performance evaluations.**Fig. 15** [Scenario#1] Static environment.**Table 2** Parameters for the static & dynamic environment.

	WCE	TurtleBot
Width	11 [mm]	$D_t = 354$ [mm]
Size of the Target Object	3 [mm]	$D_s = 3 \cdot (354/11)$ [mm]
x -coordinate of the Target	13.5 [mm]	$x_s = 13.5 \cdot (354/11)$ [mm]
y -coordinate of the Target	20.0 [mm]	$y_s = 20.0 \cdot (354/11)$ [mm]
Camera's Initial Position	-20.0 [mm]	$y_t = -20.0 \cdot (354/11)$ [mm]

the size of the TurtleBot $D_t = 0.354$ [m], therefore, the variables can be set as Table 2.

5.1.3 [Scenario#2] Target Recognition Under the Dynamic Environment

It usually takes 8 hours to go through a small intestine whose length is about 8 meters. Therefore, the average speed of the WCE \bar{V}_{WCE} can be estimated as follows:

$$\bar{V}_{WCE} = \frac{8 \text{ [m]}}{8 \text{ [hour]} \times 60 \left[\frac{\text{min}}{\text{hour}} \right] \times 60 \left[\frac{\text{sec}}{\text{min}} \right]} = \frac{1}{36} \text{ [cm/s]} \quad (7)$$

Based on it, we set the speed of the TurtleBot v_t illustrated in Fig. 16(b) as

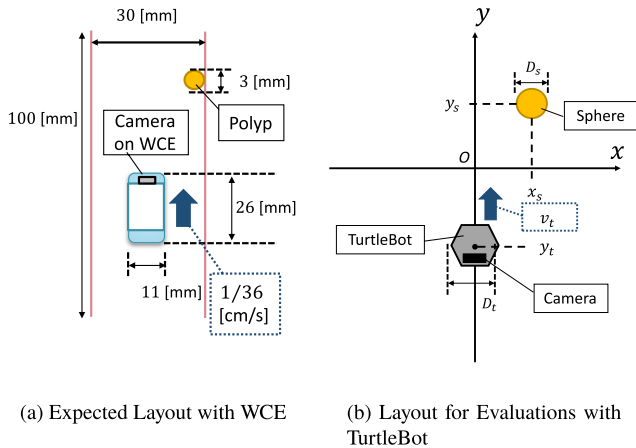


Fig. 16 [Scenario#2] Dynamic environment.

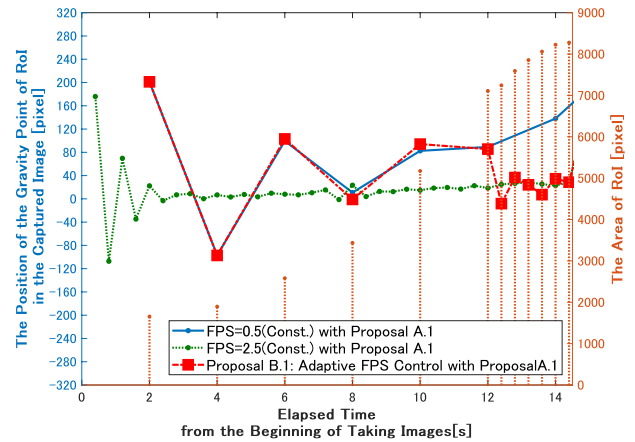


Fig. 18 A performance evaluation result for proposal B.1.

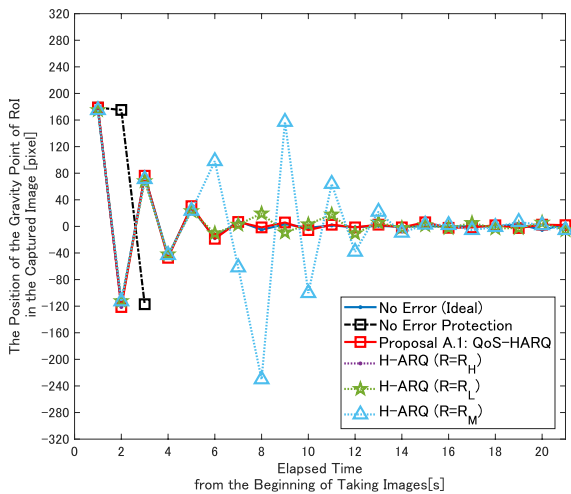


Fig. 17 A performance evaluation result for proposal A.1.

$$v_t = 10 \cdot \frac{1}{36} [\text{cm/s}] \cdot \frac{354 [\text{mm}]}{11 [\text{mm}]} = \frac{295}{33} [\text{cm/s}]. \quad (8)$$

5.2 Evaluation Results and Considerations

5.2.1 Under the Static Environment

One of the performance evaluation results for Proposal A is illustrated in Fig. 17. It shows the transition of the gravity point of Region of Interest. In the evaluation, the FPS in each scenario is set to 1 [frames/second], based on what we mentioned in 3.2, and the SNR of AWGN is set to 3 [dB].

From the figure, the proposed method shows as good target following capability as the ‘No Error (Ideal Case)’ and the ‘H-ARQ($R = R_L$).’ On the other hand, how to derive the appropriate number and value of thresholds to change the code-rate theoretically can be said as one of the issues.

5.2.2 Under the Dynamic Environment

One of the performance evaluation results for Proposal B is

illustrated in Fig. 18. In the figure, the transition of the gravity point of RoI in each scheme is also shown. In addition, the transition of the area of RoI (=the number of pixels of the RoI) with Proposal B is represented with the stem plots. In the evaluation, the SNR of AWGN is also set to be 3 [dB], and the FPS is determined based on how large the RoI is reflected in the captured image. Specifically when the area of RoI is more than 2%, the FPS is changed from 0.5 to 2.5.

From the figure, with the conventional method ‘FPS=0.5 (Const.) with Proposal A,’ it gets difficult to track the target object from 12 [s]. On the other hand, the proposed method ‘Proposal B’ achieves the adaptive capturing based on the size of RoI in the captured image. However, one of the challenging issues in the proposed method is how to prevent from missing the target object with the low frame rate.

6. Conclusion

This paper proposes the visual information based wireless feedback loop control system for the next generation wireless capsule endoscopy. From the viewpoint of constraints such as the available communication system, allowable FPS (=aFPS), under a narrow band half-duplex system, we propose the adaptive error control scheme (=Proposal A) and the adaptive delay control scheme (=Proposal B). From the performance evaluations, we could obtain insights into how to improve the recognition ratio considerably in each situation.

The future works of this research can be described as follows.

- Joint optimization of the adaptive error control and the adaptive delay control.
- Channel state/moving direction & velocity estimation with the sensing data.
- Study with full-duplex system.
- Considerations of system feasibility and system requirements.

References

- [1] K.G.N. Nair, F. Fagnani, S. Zampieri, and R.J. Evans, "Feedback control under data rate constraints: An overview," *Proc. IEEE*, vol.95, no.1, pp.108–137, Jan. 2007.
- [2] M.R. Yuce, H.C. Keong, and M.S. Chae, "Wideband communication for implantable and wearable systems," *IEEE Trans. Microw. Theory Techn.*, vol.57, no.10, pp.2597–2604, Oct. 2009.
- [3] A. Khaleghi, R. Chavez-Santiago, and I. Balasingham, "Ultra-wideband pulse-based data communications for medical implants," *IET Commun.*, vol.4, no.15, pp.1889–1897, Oct. 2010.
- [4] R. Chávez-Santiago, I. Balasingham, J. Bergsland, W. Zahid, K. Takizawa, R. Miura, and H.B. Li, "Experimental implant communication of high data rate video using an ultra wideband radio link," 2013 35th Annual International Conference of the IEEE Engineering in Medicine and Biology Society (EMBC), pp.5175–5178, July 2013.
- [5] M.R. Yuce and T. Dissanayake, "Easy-to-swallow wireless telemetry," *IEEE Microw. Mag.*, vol.13, no.6, pp.90–101, 2012.
- [6] K. Takizawa and K. Hamaguchi, "Low-complexity video encoding method for wireless image transmission in capsule endoscope," 2010 Annual International Conference of the IEEE Engineering in Medicine and Biology, pp.3479–3482, Aug. 2008.
- [7] IEEE Computer Society, "IEEE Standard for Floating-Point Arithmetic," *IEEE Std 754-2008*, pp.1–70, Aug. 2010.
- [8] S. Seimiya, K. Takabayashi, and R. Kohno, "A study for the adaptive error correction using QoS-HARQ toward dependable implant body area network," 2017 11th International Symposium on Medical Information and Communication Technology (ISMICT), pp.6–10, Feb. 2017.
- [9] K.Y. Yazdandoost, K. Sayrafian-Pour, et al., "Channel model for body area network (BAN)," *IEEE P802*, vol.15, pp.08–0780, 2009.
- [10] K. Takizawa and K. Hamaguchi, "A study on wireless video transmission from an implanted device," *IEICE Technical Report: WBS*, vol.110, no.222, pp.13–18, Sept. 2010. <https://ci.nii.ac.jp/naid/110008106900/>
- [11] *IEEE Spectrum*, "DARPA awards simulation software contact to open source robotics foundation," 2013.
- [12] S. Seimiya, K. Takabayashi, and R. Kohno, "A study for the adaptive error correction in wireless vision based feedback control under implant body area network," *IEICE Technical Report: MICT*, vol.117, no.20, pp.31–35, May 2017.
- [13] H.T. Friis, "Noise figures of radio receivers," *Proc. IRE*, vol.32, no.7, pp.419–422, July, 1944.
- [14] K. Hirai, Y. Kanazawa, R. Sagawa, and Y. Yagi, "Endoscopic image matching for reconstructing the 3-D structure of the intestines," *Medical Imaging Technology*, vol.29, no.1, pp.36–46, 2011.



Takumi Kobayashi received the B.S. and M.S. degrees in Engineering from Musashi Institute of Technology in 2011 and Tokyo City University in 2013 respectively. He received Ph.D. degree in Engineering from Yokohama National University in 2016. Currently, he is working with Center for Future Medical Social Infrastructure Based on Information Communications Technology in Yokohama National University. His research interest includes UWB communications, medical information communication technology and human body communication. He is a member of IEICE and IEEE EMBS, and a member of JSMBE.



Ryuji Kohno is IEEE and IEICE fellows. He received the Ph.D. degree in Dept.EE from the Univ. of Tokyo in 1984. Since 1998 he has been a Professor in YNU. During 1984–1985 he was a Visiting Scientist in Univ. of Toronto. Since 2007, he is also a Finnish Distinguished Professor (FiDiPro) in Univ. of Oulu, Finland. The meanwhile, he was also a director of SONY CSL/ATL during 1998–2002 and was a director of the UWB Tech. Inst. and Medical ICT Inst. of NICT during 2002–2011. Currently he is the CEO of the University of Oulu Research Institute Japan - CWC-Nippon Co. since March 2012. He was a principal leader of MEXT 21st century and Global COE programs during 2002–2007 and 2008–2013, respectively. Since 2003, he is a director of Medical ICT Center in YNU. He is an associate member of the Science Council of Japan since 2006. He was elected to be a BoG member of the IEEE Information Theory Society three times on 2000, 2002, and 2006. He was awarded IEICE Greatest Contribution Award and NTT DoCoMo Mobile Science Award in 1999 and 2002, respectively.



Satoshi Seimiya received the B.S and M.S. degrees in Engineering from Yokohama National University in 2016 and 2018 respectively. His research interest includes Ultra-reliable wireless communication, wireless feedback loop controlling, medical information communication technology and system integration. Currently, he is working with industry and contribute to development of communication technologies.